

## FAST search for circumstellar atomic hydrogen. III. Planetary nebulae at Galactic latitudes $|b| \geq 10^\circ$

XU-JIA OUYANG <sup>1</sup> YONG ZHANG <sup>1,2,3,4</sup> ALBERT ZIJLSTRA <sup>5,4</sup> CHUAN-PENG ZHANG <sup>6,7</sup>  
JUN-ICHI NAKASHIMA <sup>1,3</sup> QUENTIN A PARKER <sup>8,4,3</sup> AND XIAO-HU LI <sup>2</sup>

<sup>1</sup>*School of Physics and Astronomy, Sun Yat-sen University, 2 Daxue Road, Tangjia, Zhuhai, Guangdong Province, China*

<sup>2</sup>*Xinjiang Astronomical Observatory, Chinese Academy of Sciences, 150 Science 1-Street, Urumqi, Xinjiang 830011, People's Republic of China*

<sup>3</sup>*CSST Science Center for the Guangdong-Hongkong-Macau Greater Bay Area, Sun Yat-Sen University, Guangdong Province, China*

<sup>4</sup>*Laboratory for Space Research, The University of Hong Kong, Hong Kong, China*

<sup>5</sup>*Department of Physics and Astronomy, The University of Manchester, Manchester M13 9PL, UK*

<sup>6</sup>*National Astronomical Observatories, Chinese Academy of Sciences, Beijing 100101, China*

<sup>7</sup>*CAS Key Laboratory of FAST, National Astronomical Observatories, Chinese Academy of Sciences, Beijing 100101, China*

<sup>8</sup>*Faculty of Science, The University of Hong Kong, Chong Yuet Ming Building Pokfulam Road, Hong Kong, China*

### ABSTRACT

The detection of circumstellar atomic hydrogen (H I) via the 21 cm line remains a persistent challenge in planetary nebula (PN) studies, primarily due to contamination from ubiquitous interstellar H I 21 cm emission. In this paper, we report the results of a H I survey of 12 high surface brightness PNe located at Galactic latitudes  $|b| \geq 10^\circ$ , performed with the Five-hundred-meter Aperture Spherical radio Telescope (FAST), which is currently the most sensitive telescope in the  $L$  band. Although the contamination from interstellar emission is still severe, we detect or tentatively detect circumstellar H I 21 cm absorption associated with two PNe: NGC 6905 and NGC 7662. H I exhibits a comparatively high detection frequency in bipolar PNe. We estimate the H I masses of the two PNe to range from 0.01 to 0.14  $M_\odot$ , resulting in atomic-to-ionized hydrogen ratios of 0.02–0.3. The H I shells have dynamical ages of 2100–2400 years. Our measurements confirm previous findings that the optical depth of H I decreases with increasing linear radius of the nebula. The mass loss rates traced by the H I absorption are larger than  $10^{-5} M_\odot \text{ yr}^{-1}$ , indicating that they originate from the superwind phase at the tip of the asymptotic giant branch.

*Keywords:* Planetary nebulae (1246) — Single-dish antennas (1460) — Circumstellar envelopes (237) — Stellar mass loss (1613)

## 1. INTRODUCTION

When low- and intermediate-mass stars ( $0.8$  to  $8 M_{\odot}$ ) evolve through the asymptotic giant branch (AGB) and post-AGB phases, they eject much of their mass into the interstellar medium (ISM). Even after a significant portion of this mass has dissipated, there is a final expulsion of an envelope composed of circumstellar materials. This envelope is subsequently ionized by the central star, which has been heating up as it evolves towards becoming a white dwarf. At this particular stage, it gives rise to what is known as an optically visible planetary nebula (PN). The study of PNe greatly aids our understanding not just of late-stage stellar evolution per se but of the stellar mass feedback mechanism for galaxy evolution for the dominant low mass stellar population (see [Kwitter & Henry 2022](#), for an excellent recent review). A persistent challenge in PN research is the significant mass discrepancy between observed nebular systems and theoretical predictions. The total mass of ionized nebulae and their central stars (typically  $\leq 1.5 M_{\odot}$ , [Kimura et al. 2012](#)) falls substantially below the theoretical upper mass limit for progenitor stars. This inconsistency persists even when accounting for the faint yet extended AGB halos observed in some PNe (the so-called ‘‘PN missing mass problem’’, [Kwok 1994](#)). Extensive, deep, observations show that the combined inventory of surrounding molecules, dust, and ionized gas is insufficient to account for the mass lost by the central star when finally emerging as a PN ([Huggins et al. 1996](#); [Phillips 2007](#); [Kimura et al. 2012](#); [Andriantsaralaza et al. 2020](#); [De Marco et al. 2022](#); [Sarkar & Sahai 2022](#); [Dell’Agli et al. 2023](#)) with the ionized PN shell itself typically being only  $\sim 0.1M_{\odot}$ . Locating the missing mass has been problematic. Detecting 21 cm atomic hydrogen (H I) line<sup>1</sup> from the spin-flip transition remains exceptionally challenging in PNe. This is largely because of the considerable contamination by the omnipresent 21 cm emission of the ISM along the lines of sight in the absence of very high resolution kinematic mapping.

Investigating the complete mass loss history of a star poses significant challenges. Historically, researchers have primarily relied on CO emission in the submillimeter wavebands or dust scattering within the circumstellar envelope (CSE) to study stellar mass loss. However, these methods come with inherent limitations. For instance, CO, even in evolved stars with high mass loss rates ( $\sim 10^{-5} M_{\odot} \text{ yr}^{-1}$ ), traces scales of only  $\sim 10^4$  AU (e.g., [Saber et al. 2019](#); [Ramstedt et al. 2020](#)). Similarly, dust-scattered light covers spatial scales comparable to those traced by CO (e.g., [Mauron & Huggins 2006](#); [Mauron et al. 2013](#)). Consequently, tracers such as CO and dust do not reveal the more extended CSEs surrounding evolved stars. Interestingly, far-ultraviolet (FUV) observations have uncovered more extended structures around some AGB stars, due to interactions between molecular winds and the ISM (e.g., [Martin et al. 2007](#); [Sahai & Stenger 2023](#)). These structures are an order of magnitude larger than those traced by CO and dust ([Martin et al. 2007](#); [Sahai & Chronopoulos 2010](#); [Sahai & Mack-Crane 2014](#); [Ortiz & Guerrero 2023](#); [Sahai & Stenger 2023](#); [Guerrero & Ortiz 2024](#)). This implies that stellar mass loss extends back much further in time than can be traced by CO and dust. The luminosity observed in the FUV is thought to arise from the collisional excitation of  $\text{H}_2$  molecules by hot ( $\sim 30$  eV) electrons ([Martin et al. 2007](#); [Sahai & Chronopoulos 2010](#); [Sahai & Mack-Crane 2014](#); [Sahai & Stenger 2023](#)). According to this hypothesis, the dissociation of  $\text{H}_2$  likely results in the production of H I as a byproduct. [Glassgold & Huggins \(1983\)](#) suggest that for a photospheric temperature larger than 2500 K, the hydrogen flowing from an AGB star is mainly atomic. This has been confirmed by the detection of H I emission associated with AGB envelopes

<sup>1</sup> Throughout this paper, as a simplification, we use ‘‘H I line’’ to refer to the atomic hydrogen line at 21 cm.

(Gérard & Le Bertre 2006; Matthews et al. 2013; Gérard et al. 2024). Furthermore, during PN evolution, H I can be formed through photodissociation of  $\text{H}_2$ . Therefore, H I observations of PNe can provide significant information on their early mass-loss history. To the best of our knowledge, only five PNe, specifically IC 418, NGC 7293, BD+30°3639, KjPn 8, and NGC 6369, have been detected to date exhibiting H I 21 cm emission features (Taylor et al. 1989, 1990; Rodríguez et al. 2000, 2002; Gérard & Le Bertre 2006). Additionally, H I absorption has been observed in ten PNe (Rodríguez & Moran 1982; Altschuler et al. 1986; Schneider et al. 1987; Taylor & Pottasch 1987; Taylor et al. 1990; Gussie & Taylor 1995).

The number of PNe exhibiting circumstellar H I detections is exceedingly limited compared with the overall number of True (T), Likely (L) and Possible (P) Galactic PNe recorded in the Hong Kong/AAO/Strasbourg/H $\alpha$  PN database (HASH PN database, Parker et al. 2016) which currently stands at 3953 as at April 2025. This precludes meaningful statistical study on the relationship between the H I content and the evolution and characteristics of the associated PN. To this end, our research group has undertaken efforts to investigate H I in PNe utilizing the Five-hundred-meter Aperture Spherical radio Telescope (FAST, Nan et al. 2011), which provides the most sensitive  $L$ -band spectra of PNe to date. In Paper I (Ouyang et al. 2022), we reported the detection of a H I absorption toward IC 4997, which originates from a shell having a dynamic age of  $\sim 990$  yr. In Paper II (Ouyang et al. 2023), we reported a detection of extended H I emission surrounding the young PN BD+30°3639, which may arise from the ISM progressively swept out by the stellar wind. These results indicate that young PNe probably contain a large amount of detectable H I.

Utilizing the detection of H I absorption and emission in IC 4997 and BD+30°3639 as a reference, we have performed a search of H I in a sample of high surface brightness, mostly compact PNe. It can be considered as a development of the pioneer work of Schneider et al. (1987) at Arecibo. The more sensitive FAST observations can provide a tighter constraint on the H I mass. Section 2 describes the observations and data reduction. The results are reported in Section 3, where we estimate the masses or mass upper limits of H I. The implications of our observations on the PN evolution are discussed in Section 4, followed by the conclusions in Section 5.

## 2. OBSERVATION AND DATA REDUCTION

While PNe near the Galactic disk typically host more massive progenitors that likely harbor significant H I reservoirs, these regions suffer severe contamination from interstellar 21 cm emission. To minimize this contamination, we selected 12 high-surface-brightness PNe at Galactic latitudes  $|b| \geq 10^\circ$  (Figure 1) for observation. Table 1 lists the PNe in our sample, along with their coordinates and other parameters. Column 7 presents the distances adopted in this work. Unless otherwise specified, the distances for the sources are primarily based on Gaia DR3 parallax measurements (Chornay & Walton 2021). This step is carried out subsequent to verifying that the correct central star of the planetary nebula (CSPN) has been determined. Parker et al. (2022) have demonstrated that up to 20% of the GAIA-catalogued CSPN are misidentified. This is because a significant number of actual CSPN lie beyond the photometric limits of GAIA. Columns 8 and 9 give the angular diameters  $\theta$  and expansion velocities  $V_{\text{exp}}$  of the PN. We preferentially use the  $\theta$  values provided by the HASH PN database (Parker et al. 2016; Bojčić et al. 2021) if no other data is available. Except for those specified, the  $V_{\text{exp}}$  values are taken from Sabbadin (1984).

The observations were conducted from August 8 to November 27, 2021, using the 19-beam receiver of FAST in tracking mode. The integration time for each target varied from 40 to 50 minutes.

The 19-beam observation mode allows efficient sampling of spectra at on- and off-source positions simultaneously. Each target PN was placed in the central beam (M01), which has a half-power beamwidth of  $3'$  at 1420 MHz and a pointing accuracy standard deviation of  $7''.9$ . The surrounding beams (M02–07, see Papers I&II for the beam arrangement) sample the off-source positions about  $6'$  away from the PN in the east, south, west, and north directions. The peripheral beams (M08–19) are directed to the off-source positions about  $12'$  away from the center. The large separation between the on- and off-source positions ensures that no nebular emission is sampled in the off-position beams.

Spectra were recorded using the backend with 1,048,576 channels, resulting in a frequency resolution of 476.84 Hz, which corresponds to a velocity resolution of  $0.01 \text{ km s}^{-1}$  (Jiang et al. 2020). For flux calibration, a high-intensity noise of 12 K was periodically injected. The antenna temperature was converted to flux density using the telescope gain factor, as detailed in Section 2 of Paper II. The  $XX$  and  $YY$  linear polarization spectra were individually calibrated and baseline-subtracted. For the FAST, reflections off the dish surface and feed cabin generate standing waves that manifest as sinusoidal baselines, whereas broadband continuum emission yields polynomial-shaped baselines. We therefore selected either sinusoidal or polynomial baseline removal functions according to the specific baseline characteristics of each observation. Because the baselines are relatively smooth, their subtraction does not introduce significant uncertainty into the spectral measurements. After calibration and baseline subtraction, the  $XX$  and  $YY$  spectra were averaged to obtain the final spectra.

### 3. RESULT

Our goal is to detect H I emission and absorption features in PNe, and we name objects displaying such spectral signatures as HIPNe. If a feature at a right velocity appears in the on-source spectrum but is invisible in all the off-source spectra, we can consider it to potentially be of PN origin. However, this approach is only feasible when the interstellar emission varies smoothly across the beams. Otherwise, interferometric observations are more suitable to filter out the interstellar emission. Nevertheless, the single-dish observation provides an efficient way to search for HIPN candidates.

Figure 2 shows that the contamination from interstellar H I emission is still significant for most of the PNe, largely hindering the detection of circumstellar H I. Nevertheless, the systemic velocities of NGC 3587 and NGC 6852 differ significantly from those of interstellar H I foreground. This allows us to derive a tight upper limit of the flux density for the 21 cm line flux density ( $S_{\text{line}}$ ) in the two PNe, based on the RMS of their spectra ( $S_{\text{line}} = \text{RMS}$ ). For the other PNe,  $S_{\text{line}}$  is derived from the flux-density standard deviation of the M02–07 off-source spectra.

#### 3.1. *H I absorption*

Atomic hydrogen occupies the interface between the ionized and molecular regions of PNe, where the radiation field from the central star is not hard enough to ionize H but can significantly dissociate  $\text{H}_2$ . The free-free emission arising from inner ionized nebulae provides the emission continuum at L band against which the 21 cm H I absorption could be measured blueward of the systemic velocity of the expanding ionized nebulae.

For spatially resolved PNe, the optical emission line profiles typically exhibit two split components. The blue-shifted component represents the part of the expanding nebula moving towards the observer, while the red-shifted component represents the part moving away. The [N II] lines at 6548 and 6584 Å can be used to trace the velocity of the outermost ionized gas, which can be accelerated by

the pressure of the ionized gas. Apart from [N II] lines, the kinematic of the ionized gas's outer layers may also be traced by the velocity span of H $\alpha$  line (Acker et al. 2002). We gathered the profiles of the [N II] lines in the SPM Kinematic Catalogue of Galactic Planetary Nebulae<sup>2</sup> (López et al. 2012) which covers many Galactic PNe of high surface brightness such as for this sample. [N II] lines of NGC 2022 and NGC 6852 were unavailable in the SPM catalogue, and thus we examined H $\alpha$  line instead. The catalogue does not include IC 4846. As discussed in Paper II, the [N II] lines trace the outermost ionized gas, which is spatially close to the neutral shell. Therefore, the circumstellar H I absorption feature should be located on a position close to the blue end of the [N II] and H $\alpha$  lines.

As shown in Figure 2, although interstellar H I emission is strong, we tentatively detect circumstellar H I absorption in NGC 6905 and NGC 7662. Taken the flux densities of the continuum emission at 21 cm ( $S_{21 \text{ cm}}$ ) from the literature<sup>3</sup> (as listed in column 4 of Table 2), we can derive the integrated optical depth using  $\int \tau_v dv = -\int S_{\text{HI}} dv / S_{21 \text{ cm}}$ , where  $S_{\text{HI}}$  is the flux densities of the 21 cm line subtracted by  $S_{21 \text{ cm}}$ . For non-detections, the upper limits of  $|S_{\text{HI}}|$  can be estimated from  $S_{\text{line}}$ . Table 2 presents  $\int S_{\text{line}} dv$  and the resultant  $\int \tau_v dv$  upper limits in non-HIPNe. The circumstellar H I absorption in HIPNe is measured through a Gaussian profile fitting, and the results are presented in Table 3. Based on the measured expansion velocities, angular radii, and distances, we determined the dynamic ages of the H I shells are 2100 and 2400 years in NGC 6905 and NGC 7662, respectively.

The H I mass associated with the 21 cm absorption can be obtained by the following formula:

$$M_{\text{ab}} = 2.14 \times 10^{-6} \Gamma \left( \frac{T_{\text{ex}}}{\text{K}} \right) \left( \frac{D}{\text{kpc}} \right)^2 \left( \frac{\theta}{''} \right)^2 \left( \frac{\int \tau_v dv}{\text{km s}^{-1}} \right) M_{\odot}, \quad (1)$$

where  $\Gamma$  is the geometric factor that accounts for atomic gases that are not in the line of sight,  $T_{\text{ex}}$  is the spin-excitation temperature, and  $D$  is the distance. For the calculations, we simply assume  $\Gamma = 1$  and  $T_{\text{ex}} = 100 \text{ K}$  (see Paper I for a discussion of the assumptions). If the atomic gas is close to the ionization front,  $T_{\text{ex}}$  approaches to 1000 K, and  $M_{\text{ab}}$  would be underestimated by a factor of ten. If the atomic gas is distributed in the outer layers, similar in scale to H<sub>2</sub> (e.g.  $\sim 2$  times the size of ionized regions),  $\Gamma$  is 4, and  $M_{\text{ab}}$  would be underestimated by a factor of four. As a result, the upper limits of  $M_{\text{ab}}$  range from 0.001  $M_{\odot}$  to 16.2  $M_{\odot}$ .  $M_{\text{ab}}$  in HIPNe lies in a range of 0.01–0.14  $M_{\odot}$ , which encompasses the value of IC 4997 (Paper I).

### 3.2. H I emission

Following the approach outlined in Papers I and II, we search for H I emission by comparing the ‘ON-OFF’ and ‘OFF-OFF’ spectra. The off-position spectrum for primary comparison was obtained by averaging beam samples from positions M02–M07 (surrounding M01). Additionally, we generated two independent reference spectra by separately averaging the east–west and north–south beams. However, we did not detect apparent H I emission associated with the PNe. The mass upper limits of circumstellar H I can be estimated from  $S_{\text{line}}$  using the formula:

$$M_{\text{em}} = 2.36 \times 10^{-4} \left( \frac{D}{\text{kpc}} \right)^2 \left( \frac{\int S_{\text{line}} dv}{\text{mJy km s}^{-1}} \right) M_{\odot}, \quad (2)$$

<sup>2</sup> <http://kincatpn.astrosen.unam.mx>

<sup>3</sup> Our observation setup was optimized for spectral line observations. The ON- and OFF-source spectra were acquired using different beams, introducing significant uncertainty in measuring the continuum emission. Additionally, the baseline may include both continuum emission and standing wave artifacts, prompting our reliance on literature-derived flux density values for subsequent analysis.

as listed in Column 8 of Table 2. For comparison, we computed the mass of the ionized gas through

$$M_i = 5.34 \times 10^{-5} \left( \frac{D}{\text{kpc}} \right)^{5/2} \left( \frac{\theta}{''} \right)^{3/2} \left( \frac{S_{6 \text{ cm}}}{\text{mJy}} \right) M_\odot, \quad (3)$$

where  $S_{6 \text{ cm}}$  is the continuum emission at 6 cm dominated by free-free emission. The derived  $M_i$  values is listed in the column 10 of Table 2, which ranges from 0.005 to  $1.9 M_\odot$ . Most of the PNe have  $M_{\text{em}}$  of less than  $1 M_\odot$ . The tightest limit is that of NGC 3578, in which  $M_{\text{em}} < 0.004 M_\odot$  and the mass ratio of atomic to ionized gas is less than 0.01.

In line with the cases of other PNe, H I emission was not detected in the two HIPNe. Table 4 presents the mass of the ionized gas and the upper limits of the H I emission gas in the HIPNe, as well as their morphological classifications<sup>4</sup>. In principle, a comparison between  $M_{\text{em}}$  and  $M_{\text{ab}}$  could yield insights into the spatial extent of the H I shell. However, the upper limits established for  $M_{\text{em}}$  exceed the  $M_{\text{ab}}$  values, precluding meaningful conclusions from this comparison.

#### 4. DISCUSSION

The results allow us to investigate the ‘PN mass missing problem’. As pointed out by Frew et al. (2012), the PN progenitor star has a typical mass of  $2.5 M_\odot$ . After the superwind phase, the mass of the residual white dwarf is typically only  $0.6 M_\odot$ . Our results suggest that in general the mass of H I gas are less or comparable with  $M_i$ . The upper limits of the total mass of ionized and atomic gas (based on H I emission) are less than  $\sim 2 M_\odot$  with a median value of  $0.9 M_\odot$ . The mass ratios of atomic to ionized gas in NGC 6905 and NGC 7662 are 0.3 and 0.02, respectively. Therefore, the atomic gas cannot account for all the missing mass of PNe.

It is conceivable that the optical depth of the neutral envelope increases with increasing mass loss rate ( $\dot{M}$ ) and decreases with nebular expansion. According to Taylor et al. (1990), they satisfy a relation of

$$\int \tau_v dv = 3.8 \times 10^6 \frac{\dot{M}}{T_{\text{ex}} \mu v_n r_i} \left( 1 - \frac{r_i}{r_n} \right) \text{ km s}^{-1}, \quad (4)$$

where  $\mu$  is the mean molecular weight,  $v_n$  is the expansion velocity of the neutral shell, and  $r_i$  and  $r_n$  are the radii of the ionized and neutral shells, respectively. Assuming  $r_n \gg r_i$ ,  $v_n = 10 \text{ km s}^{-1}$ , and  $T_{\text{ex}} = 100 \text{ K}$ , we calculate  $\int \tau_v dv$  as functions of  $r_i$  for  $\dot{M} = 10^{-6}$ ,  $10^{-5}$ , and  $10^{-4} M_\odot \text{ yr}^{-1}$ , as indicated in Figure 3. Table 5 lists all the PNe or which circumstellar H I absorption has been detected in the existing literature, along with their respective characteristics. Here,  $r_i$  is calculated by employing the updated distance values. As shown in Figure 3, the observational results are consistent with the theoretical predictions, and indicate a mass loss rate of  $10^{-6}$ – $10^{-4} M_\odot \text{ yr}^{-1}$  that is systematically higher than those obtained by Taylor et al. (1990) and Gussie & Taylor (1995). The high mass loss rates suggest that the H I shell may be generated in the superwind epoch at the tip of the AGB.

Our analysis of HIPNe (Tables 4 & 5) reveals that 69% (9 out of 13) exhibit bipolar morphologies (as classified in HASH). This proportion is notably higher than the approximately  $\sim 20\%$  bipolar fraction observed in the general PN population (e.g., HASH; Sahai et al. 2011). This correlation suggests a potential connection between bipolarity and enhanced H I detectability.

<sup>4</sup> The morphological classifications were adopted from the HASH database (Parker et al. 2006), which follows the classification scheme proposed by Corradi & Schwarz (1995). PNe are mainly categorized as Elliptical or oval (E), Round (R), Bipolar (B), Irregular (I), Asymmetric (A), or quasi-Stellar or point source (S) under the ‘ERBIAS’ classifier. An additional ‘amprs’ subclassifier is used to denote specific features, namely asymmetric enhancement (a), multiple shells (m), point-symmetry (p), ring structure or annulus (r), or resolved internal structure (s). Each PN is assigned one primary classification and may have multiple subclassifiers, which are listed in alphabetical order.

The majority of prior detections of HIPNe have relied on single-dish observations, which lack sufficient spatial resolution to resolve H I structure. In contrast, interferometric observations of NGC 6302 reveal that its H I emission originates in a dust-shielded torus (Rodriguez et al. 1985), suggesting that such circumstellar tori may protect neutral hydrogen from ionization. Importantly, all HIPNe exhibit bright radio continuum emission in the NRAO VLA Sky Survey (NVSS) (Condon & Kaplan 1998), a feature that provides a robust background for H I absorption measurements and thereby enhances detection sensitivity.

## 5. CONCLUSION

Using FAST, we conducted a H I survey of 12 high surface brightness PNe at relatively high Galactic latitudes. The detection rate of HIPNe remains low due to either contamination from interstellar H I emission or morphological selection bias in PN sample. We report tentative detections of circumstellar H I absorption in NGC 6905 and NGC 7662. The mass of atomic gas in the two PNe ranges from 0.01 to  $0.14 M_\odot$ , resulting in a mass ratio of atomic to ionized gas of 0.02–0.3.

Nevertheless, our observations place tight upper limits for the H I mass in PNe, in particularly for those with  $V_{\text{LSR}}$  substantially differing from the velocity of interstellar H I lines. We show that the mass of atomic gas in PNe is unlikely to be higher than that of ionized mass, and thus the ‘PN mass missing problem’ persists.

Furthermore, we confirm previous findings that the H I absorption fades away with PN evolution. The high mass loss rate implied by the observations suggests that the H I shell may origin from a superwind epoch at the termination of AGB evolution.

The discovery of more HIPNe, strongly dominated by specific bipolar morphologies, is necessary to build a statistically significant sample to study the neutral shell of PNe. Although interferometric observations has certain advantage of filtering out large-scale interstellar H I emission, sensitive single-dish observations such as FAST can offer a practical means of identifying HIPN candidates. For that, we need to observe PNe with the line-of-sight velocity significantly different from the Galactic rotation curve.

## ACKNOWLEDGEMENTS

We would like to express our sincere gratitude to the two anonymous reviewers for their insightful suggestions, which have significantly enhanced the quality of this paper. The financial supports of this work are from the National Natural Science Foundation of China (NSFC, No. 12473027 and 12333005), the Guangdong Basic and Applied Basic Research Funding (No. 2024A1515010798), and the science research grants from the China Manned Space Project (NO. CMS-CSST-2021-A09, CMS-CSST-2021-A10, etc). Y.Z. thanks the Xinjiang Tianchi Talent Program (2023). X.H.L. acknowledges support from the Natural Science Foundation of Xinjiang Uygur Autonomous Region (No. 2024D01E37) and the National Science Foundation of China (12473025). Q.A.P. thanks the Hong Kong Research Grants Council for GRF research support under grants 17326116 and 17300417. This work made use of the data from FAST (Five-hundred-meter Aperture Spherical radio Telescope). FAST is a Chinese national mega-science facility, operated by National Astronomical Observatories, Chinese Academy of Sciences.

## REFERENCES

- Aaquist, O. B., & Kwok, S. 1990, *A&AS*, 84, 229
- Acker, A., Gesicki, K., Grosdidier, Y., & Durand, S. 2002, *A&A*, 384, 620,  
doi: [10.1051/0004-6361:20020009](https://doi.org/10.1051/0004-6361:20020009)

- Ali, A., & Alharbi, W. R. 2021, *Research in Astronomy and Astrophysics*, 21, 151, doi: [10.1088/1674-4527/21/6/151](https://doi.org/10.1088/1674-4527/21/6/151)
- Altschuler, D. R., Schneider, S. E., Giovanardi, C., & Silverglate, P. R. 1986, *ApJL*, 305, L85, doi: [10.1086/184690](https://doi.org/10.1086/184690)
- Andriantsaralaza, M., Zijlstra, A., & Avison, A. 2020, *MNRAS*, 491, 758, doi: [10.1093/mnras/stz3026](https://doi.org/10.1093/mnras/stz3026)
- Becker, R. H., White, R. L., & Edwards, A. L. 1991, *ApJS*, 75, 1, doi: [10.1086/191529](https://doi.org/10.1086/191529)
- Bianchi, L. 1992, *A&A*, 260, 314
- Bojičić, I. S., Filipović, M. D., Urošević, D., Parker, Q. A., & Galvin, T. J. 2021, *MNRAS*, 503, 2887, doi: [10.1093/mnras/stab687](https://doi.org/10.1093/mnras/stab687)
- Chornay, N., & Walton, N. A. 2021, *A&A*, 656, A110, doi: [10.1051/0004-6361/202142008](https://doi.org/10.1051/0004-6361/202142008)
- Condon, J. J., & Kaplan, D. L. 1998, *ApJS*, 117, 361, doi: [10.1086/313128](https://doi.org/10.1086/313128)
- Condon, J. J., Kaplan, D. L., & Terzian, Y. 1999, *ApJS*, 123, 219, doi: [10.1086/313236](https://doi.org/10.1086/313236)
- Corradi, R. L. M., & Schwarz, H. E. 1995, *A&A*, 293, 871
- De Marco, O., Crowther, P. A., Barlow, M. J., Clayton, G. C., & de Koter, A. 2001, *MNRAS*, 328, 527, doi: [10.1046/j.1365-8711.2001.04887.x](https://doi.org/10.1046/j.1365-8711.2001.04887.x)
- De Marco, O., Akashi, M., Akras, S., et al. 2022, *Nature Astronomy*, 6, 1421, doi: [10.1038/s41550-022-01845-2](https://doi.org/10.1038/s41550-022-01845-2)
- Dell'Agli, F., Tosi, S., Kamath, D., et al. 2023, *MNRAS*, 526, 5386, doi: [10.1093/mnras/stad3080](https://doi.org/10.1093/mnras/stad3080)
- Frew, D. J., Bojičić, I. S., & Parker, Q. A. 2012, in *IAU Symposium*, Vol. 283, *Planetary Nebulae: An Eye to the Future*, 362–363, doi: [10.1017/S174392131201143X](https://doi.org/10.1017/S174392131201143X)
- Frew, D. J., Parker, Q. A., & Bojičić, I. S. 2016, *MNRAS*, 455, 1459, doi: [10.1093/mnras/stv1516](https://doi.org/10.1093/mnras/stv1516)
- Gathier, R., Pottasch, S. R., & Goss, W. M. 1986, *A&A*, 157, 191
- Gérard, E., & Le Bertre, T. 2006, *AJ*, 132, 2566, doi: [10.1086/508811](https://doi.org/10.1086/508811)
- Gérard, E., van Driel, W., Matthews, L. D., et al. 2024, *A&A*, 692, A54, doi: [10.1051/0004-6361/202451744](https://doi.org/10.1051/0004-6361/202451744)
- Glassgold, A. E., & Huggins, P. J. 1983, *MNRAS*, 203, 517, doi: [10.1093/mnras/203.2.517](https://doi.org/10.1093/mnras/203.2.517)
- Gómez, J. F., Suárez, O., Gómez, Y., et al. 2008, *AJ*, 135, 2074, doi: [10.1088/0004-6256/135/6/2074](https://doi.org/10.1088/0004-6256/135/6/2074)
- Guerrero, M. A., & Ortiz, R. 2024, *MNRAS*, 527, 4730, doi: [10.1093/mnras/stad3458](https://doi.org/10.1093/mnras/stad3458)
- Gussie, G. T., & Taylor, A. R. 1995, *MNRAS*, 273, 801, doi: [10.1093/mnras/273.3.801](https://doi.org/10.1093/mnras/273.3.801)
- HI4PI Collaboration, Ben Bekhti, N., Flöer, L., et al. 2016, *A&A*, 594, A116, doi: [10.1051/0004-6361/201629178](https://doi.org/10.1051/0004-6361/201629178)
- Huggins, P. J., Bachiller, R., Cox, P., & Forveille, T. 1996, *A&A*, 315, 284
- Jacoby, G. H., & Chu, Y. H. 1989, in *Planetary Nebulae*, ed. S. Torres-Peimbert, Vol. 131, 183
- Jiang, P., Tang, N.-Y., Hou, L.-G., et al. 2020, *Research in Astronomy and Astrophysics*, 20, 064, doi: [10.1088/1674-4527/20/5/64](https://doi.org/10.1088/1674-4527/20/5/64)
- Kimura, R. K., Gruenwald, R., & Aleman, I. 2012, *A&A*, 541, A112, doi: [10.1051/0004-6361/201118429](https://doi.org/10.1051/0004-6361/201118429)
- Kwitter, K. B., & Henry, R. B. C. 2022, *PASP*, 134, 022001, doi: [10.1088/1538-3873/ac32b1](https://doi.org/10.1088/1538-3873/ac32b1)
- Kwok, S. 1994, *PASP*, 106, 344, doi: [10.1086/133384](https://doi.org/10.1086/133384)
- López, J.-A., Richer, M. G., García-Díaz, M.-T., et al. 2012, *IAU Symposium*, 283, 63, doi: [10.1017/S1743921312010708](https://doi.org/10.1017/S1743921312010708)
- Luri, X., Brown, A. G. A., Sarro, L. M., et al. 2018, *A&A*, 616, A9, doi: [10.1051/0004-6361/201832964](https://doi.org/10.1051/0004-6361/201832964)
- Martin, D. C., Seibert, M., Neill, J. D., et al. 2007, *Nature*, 448, 780, doi: [10.1038/nature06003](https://doi.org/10.1038/nature06003)
- Matthews, L. D., Le Bertre, T., Gérard, E., & Johnson, M. C. 2013, *AJ*, 145, 97, doi: [10.1088/0004-6256/145/4/97](https://doi.org/10.1088/0004-6256/145/4/97)
- Mauron, N., & Huggins, P. J. 2006, *A&A*, 452, 257, doi: [10.1051/0004-6361:20054739](https://doi.org/10.1051/0004-6361:20054739)
- Mauron, N., Huggins, P. J., & Cheung, C. L. 2013, *A&A*, 551, A110, doi: [10.1051/0004-6361/201219517](https://doi.org/10.1051/0004-6361/201219517)
- Meatheringham, S. J., Wood, P. R., & Faulkner, D. J. 1988, *ApJ*, 334, 862, doi: [10.1086/166882](https://doi.org/10.1086/166882)
- Milne, D. K. 1979, *A&AS*, 36, 227
- Morisset, C., & Georgiev, L. 2009, *A&A*, 507, 1517, doi: [10.1051/0004-6361/200912413](https://doi.org/10.1051/0004-6361/200912413)
- Nan, R., Li, D., Jin, C., et al. 2011, *International Journal of Modern Physics D*, 20, 989, doi: [10.1142/S0218271811019335](https://doi.org/10.1142/S0218271811019335)
- Ortiz, R., & Guerrero, M. A. 2023, *MNRAS*, 522, 811, doi: [10.1093/mnras/stad984](https://doi.org/10.1093/mnras/stad984)
- Ouyang, X.-J., Zhang, Y., Zijlstra, A., et al. 2022, *ApJ*, 933, 4, doi: [10.3847/1538-4357/ac6fdb](https://doi.org/10.3847/1538-4357/ac6fdb)

- . 2023, *ApJ*, 952, 166,  
doi: [10.3847/1538-4357/acd761](https://doi.org/10.3847/1538-4357/acd761)
- Parker, Q. A., Bojičić, I. S., & Frew, D. J. 2016,  
in *Journal of Physics Conference Series*, Vol.  
728, *Journal of Physics Conference Series*,  
032008, doi: [10.1088/1742-6596/728/3/032008](https://doi.org/10.1088/1742-6596/728/3/032008)
- Parker, Q. A., Xiang, Z., & Ritter, A. 2022,  
*Galaxies*, 10, 32, doi: [10.3390/galaxies10010032](https://doi.org/10.3390/galaxies10010032)
- Parker, Q. A., Acker, A., Frew, D. J., et al. 2006,  
*MNRAS*, 373, 79,  
doi: [10.1111/j.1365-2966.2006.10950.x](https://doi.org/10.1111/j.1365-2966.2006.10950.x)
- Phillips, J. P. 2007, *MNRAS*, 381, 117,  
doi: [10.1111/j.1365-2966.2007.12199.x](https://doi.org/10.1111/j.1365-2966.2007.12199.x)
- Pottasch, S. R., & Surendiranath, R. 2005, *A&A*,  
432, 139, doi: [10.1051/0004-6361:20042006](https://doi.org/10.1051/0004-6361:20042006)
- Ramstedt, S., Vlemmings, W. H. T., Doan, L.,  
et al. 2020, *A&A*, 640, A133,  
doi: [10.1051/0004-6361/201936874](https://doi.org/10.1051/0004-6361/201936874)
- Rodríguez, L. F., Gómez, Y., & López, J. A. 2000,  
*RMxAA*, 36, 51
- Rodríguez, L. F., Goss, W. M., & Williams, R.  
2002, *ApJ*, 574, 179, doi: [10.1086/340800](https://doi.org/10.1086/340800)
- Rodríguez, L. F., & Moran, J. M. 1982, *Nature*,  
299, 323, doi: [10.1038/299323a0](https://doi.org/10.1038/299323a0)
- Rodríguez, L. F., Garcia-Barreto, J. A., Canto, J.,  
et al. 1985, *MNRAS*, 215, 353,  
doi: [10.1093/mnras/215.3.353](https://doi.org/10.1093/mnras/215.3.353)
- Sabbadin, F. 1984, *A&AS*, 58, 273
- Saberi, M., Vlemmings, W. H. T., & De Beck, E.  
2019, *A&A*, 625, A81,  
doi: [10.1051/0004-6361/201935309](https://doi.org/10.1051/0004-6361/201935309)
- Sahai, R., & Chronopoulos, C. K. 2010, *ApJL*,  
711, L53, doi: [10.1088/2041-8205/711/2/L53](https://doi.org/10.1088/2041-8205/711/2/L53)
- Sahai, R., & Mack-Crane, G. P. 2014, *AJ*, 148, 74,  
doi: [10.1088/0004-6256/148/4/74](https://doi.org/10.1088/0004-6256/148/4/74)
- Sahai, R., Morris, M. R., & Villar, G. G. 2011,  
*AJ*, 141, 134, doi: [10.1088/0004-6256/141/4/134](https://doi.org/10.1088/0004-6256/141/4/134)
- Sahai, R., & Stenger, B. 2023, *AJ*, 165, 229,  
doi: [10.3847/1538-3881/acccf2](https://doi.org/10.3847/1538-3881/acccf2)
- Santander-García, M., Jones, D., Alcolea, J.,  
Bujarrabal, V., & Wesson, R. 2022, *A&A*, 658,  
A17, doi: [10.1051/0004-6361/202142233](https://doi.org/10.1051/0004-6361/202142233)
- Sarkar, G., & Sahai, R. 2022, *ApJ*, 940, 54,  
doi: [10.3847/1538-4357/ac8d03](https://doi.org/10.3847/1538-4357/ac8d03)
- Schneider, S. E., Silverglate, P. R., Altschuler,  
D. R., & Giovanardi, C. 1987, *ApJ*, 314, 572,  
doi: [10.1086/165086](https://doi.org/10.1086/165086)
- Schneider, S. E., Terzian, Y., Purgathofer, A., &  
Perinotto, M. 1983, *ApJS*, 52, 399,  
doi: [10.1086/190874](https://doi.org/10.1086/190874)
- Taylor, A. R., Gussie, G. T., & Goss, W. M. 1989,  
*ApJ*, 340, 932, doi: [10.1086/167447](https://doi.org/10.1086/167447)
- Taylor, A. R., Gussie, G. T., & Pottasch, S. R.  
1990, *ApJ*, 351, 515, doi: [10.1086/168489](https://doi.org/10.1086/168489)
- Taylor, A. R., & Pottasch, S. R. 1987, *A&A*, 176,  
L5
- Vickers, S. B., Frew, D. J., Parker, Q. A., &  
Bojičić, I. S. 2015, *MNRAS*, 447, 1673,  
doi: [10.1093/mnras/stu2383](https://doi.org/10.1093/mnras/stu2383)
- Weinberger, R. 1989, *A&AS*, 78, 301

**Table 1.** PN sample selected for the present work.

Name	RA	DEC	$l$	$b$	$V_{\text{LSR}}$	$D^d$	$\theta$	$V_{\text{exp}}$
	(h m s)	( $^{\circ}$ ' ")	( $^{\circ}$ )	( $^{\circ}$ )	(km s $^{-1}$ )	kpc	"	(km s $^{-1}$ )
(1)	(2)	(3)	(4)	(5)	(6)	(7)	(8)	(9)
NGC 650-1	01h42m19.66s	+51d34m31.6s	130.9	-10.5	-16.1 $\pm$ 1.2 <sup>a</sup>	0.93 $\pm$ 0.26 <sup>e</sup>	84.00 <sup>f</sup>	38.5
NGC 2022	05h42m06.19s	+09d05m10.9s	196.7	-10.9	-1.3 $\pm$ 2.2 <sup>a</sup>	2.27 <sup>+0.29</sup> <sub>-0.23</sub>	23.22 <sup>g</sup>	27.5
Abell 21	07h29m02.88s	+13d14m30.0s	205.1	+14.2	15.4 $\pm$ 5.2 <sup>a</sup>	0.59 <sup>+0.03</sup> <sub>-0.02</sub>	375.00 <sup>f</sup>	32.0 <sup>h</sup>
Abell 30	08h46m54.40s	+17d52m32.6s	208.6	+33.3	0.9 <sup>b</sup>	2.22 <sup>+0.16</sup> <sub>-0.14</sub>	63.50 <sup>f</sup>	40.0
NGC 3587	11h14m47.71s	+55d01m08.5s	148.5	+57.0	11.5 $\pm$ 3.1 <sup>a</sup>	0.81 <sup>+0.03</sup> <sub>-0.03</sub>	104.00 <sup>f</sup>	30.0
Hu 2-1	18h49m47.57s	+20d50m39.5s	51.5	+9.7	33.0 $\pm$ 3.1 <sup>a</sup>	2.38 <sup>+0.48</sup> <sub>-0.34</sub>	2.06 <sup>g</sup>	10.0
IC 4846	19h16m28.22s	-09d02m36.8s	27.6	-9.6	165.7 $\pm$ 3.0 <sup>a</sup>	7.13 $\pm$ 2.01 <sup>e</sup>	2.93 <sup>g</sup>	13.1 <sup>i</sup>
NGC 6826	19h44m48.15s	+50d31m30.2s	83.6	+12.8	10.9 $\pm$ 0.6 <sup>a</sup>	1.30 <sup>+0.07</sup> <sub>-0.06</sub>	21.96 <sup>g</sup>	8.0
NGC 6852	20h00m39.21s	+01d43m40.9s	42.6	-14.5	-3.1 <sup>c</sup>	2.56 <sup>+1.14</sup> <sub>-0.60</sub>	1.67 <sup>g</sup>	43.1 <sup>h</sup>
NGC 6891	20h15m08.84s	+12d42m15.6s	54.2	-12.1	58.6 $\pm$ 1.0 <sup>a</sup>	2.56 <sup>+0.21</sup> <sub>-0.18</sub>	9.91 <sup>g</sup>	10.0
NGC 6905	20h22m22.99s	+20d06m16.3s	61.5	-9.6	8.1 $\pm$ 1.7 <sup>a</sup>	2.70 <sup>+0.24</sup> <sub>-0.20</sub>	21.65 <sup>f</sup>	43.5
NGC 7662	23h25m53.60s	+42d32m06.0s	106.6	-17.6	-4.7 $\pm$ 0.7 <sup>a</sup>	1.75 <sup>+0.10</sup> <sub>-0.09</sub>	23.42 <sup>g</sup>	26.5

NOTE—<sup>a</sup> Schneider et al. (1983); <sup>b</sup> Jacoby & Chu (1989); <sup>c</sup> Meatheringham et al. (1988); <sup>d</sup> Chornay & Walton (2021); <sup>e</sup> Frew et al. (2016); <sup>f</sup> HASH; <sup>g</sup> Bojčić et al. (2021); <sup>h</sup> Ali & Alharbi (2021); <sup>i</sup> Bianchi (1992).

**Table 2.** Spectroscopic measurements and upper mass limits of H I in the non-HIPNe.

Name	rms	Devi	$S_{21\text{cm}}^b$	$S_6\text{cm}$	$\int S_{\text{line}} dv$	$\int \tau_v dv$	$M_{\text{em}}$	$M_{\text{ab}}$	$M_i$
	(mJy)	(mJy)	(mJy)	(mJy)	(mJy km s $^{-1}$ )	(km s $^{-1}$ )	( $M_{\odot}$ )	( $M_{\odot}$ )	( $M_{\odot}$ )
(1)	(2)	(3)	(4)	(5)	(6)	(7)	(8)	(9)	(10)
NGC 650-1	0.74	34.44	141.1 $\pm$ 4.9	117 <sup>d</sup>	1414.5	10.0	<0.3	<3.3	0.4
NGC 2022	0.93	51.51	93.2 $\pm$ 3.8	80 <sup>d</sup>	1511.1	16.2	<1.8	<2.4	0.4
Abell 21	0.33	15.40	>85 <sup>c</sup>	327 <sup>e</sup>	525.7	<6.2	<0.04	<16.2	1.9
Abell 30	0.77	5.50	<5	...	234.7	>46.9	...	...	...
NGC 3587	0.74	0.42	115.9 $\pm$ 6.8	88 <sup>d</sup>	23.68	0.2	<0.004	<0.08	0.3
Hu 2-1 <sup>a</sup>	1.58	121.53	43.0 $\pm$ 1.4	110 <sup>f</sup>	1296.4	30.1	<1.7	<0.04	0.01
IC 4846	0.48	1.2	40.7 $\pm$ 1.6	43 <sup>e</sup>	16.7	0.4	<0.2	<0.01	0.2
NGC 6826	0.77	4.46	415.0 $\pm$ 16.0	373 <sup>d</sup>	38.1	0.1	<0.02	<0.004	0.2
NGC 6852	0.34	1.04	13.5 $\pm$ 1.5	20 <sup>e</sup>	15.63	1.2	<0.02	<0.001	0.005
NGC 6891	1.88	61.77	111.3 $\pm$ 3.4	109 <sup>d</sup>	658.9	5.9	<1.0	<0.2	0.2

NOTE—<sup>a</sup> Gussie & Taylor (1995) reported tentative H I detection in this bipolar PN. However, in the present work, the detection of H I is significantly obstructed by the substantial contamination of interstellar H I emission. <sup>b</sup> Condon & Kaplan (1998); <sup>c</sup> Condon et al. (1999); <sup>d</sup> Becker et al. (1991); <sup>e</sup> Milne (1979); <sup>f</sup> Aaquist & Kwok (1990).

**Table 3.** Measurements of the H I absorption and H I masses in the HIPNe.

Name	$S_{21\text{cm}}^a$	$\int S_{\text{HI}} dv$	$V_{\text{HI}}$	FWHM	$S_p$	$\int \tau_v dv$	$M_{\text{ab}}$	$V_{\text{exp}}$
	(mJy)	(mJy km s $^{-1}$ )	(km s $^{-1}$ )	(km s $^{-1}$ )	(mJy)	(km s $^{-1}$ )	( $M_\odot$ )	(km s $^{-1}$ )
(1)	(2)	(3)	(4)	(5)	(6)	(7)	(8)	(9)
NGC 6905	$67.3 \pm 2.7$	$-50.40 \pm 5.59$	$-40.75 \pm 1.67$	$33.91 \pm 4.74$	$-1.40 \pm 0.12$	$0.75 \pm 0.15$	0.14	65.80
NGC 7662	$646.0 \pm 19.0$	$-61.78 \pm 9.34$	$-32.52 \pm 1.51$	$24.39 \pm 4.74$	$-2.38 \pm 0.25$	$0.10 \pm 0.18$	0.01	40.01

**Table 4.** Ionized gas masses and  $M_{\text{em}}$  upper limits in the HIPNe.

Name	rms	Devi	$S_{6\text{cm}}$	$\int S_{\text{line}} dv$	$M_{\text{em}}$	$M_i$	Morph.
	(mJy)	(mJy)	(mJy)	(mJy km s $^{-1}$ )	( $M_\odot$ )	( $M_\odot$ )	
(1)	(2)	(3)	(4)	(5)	(6)	(7)	(8)
NGC 6905	0.34	2.31	$63^a$	107.2	$<0.18$	0.51	Bmps
NGC 7662	0.46	12.06	$605^a$	340.9	$<0.25$	0.60	Emrs

NOTE—<sup>a</sup> Becker et al. (1991).**Table 5.** Catalog of HIPNe from the literature.

Name	$l$	$b$	Distance	$\theta^l$	$r_i$	$\int \tau_v dv$	Morph.
	$^\circ$	$^\circ$	(kpc)	( $''$ )	(pc)	(km s $^{-1}$ )	
(1)	(2)	(3)	(4)	(5)	(6)	(7)	(8)
NGC 6302	349.51	+1.06	$1.17^a$	17.77	0.05	$3.5 \pm 0.4^n$	Bamps
NGC 6790	037.89	-6.31	$0.8^b$	2.18	0.04	$1.5 \pm 0.12^o$	Bps
NGC 6886	60.14	-7.73	$2.6^c$	4.09	0.03	$0.87 \pm 0.12^o$	Bmps
IC 418	215.21	-24.28	$1.26^d$	13.08	0.04	$0.16 \pm 0.03^o$	Emrs
IC 5117	89.87	-5.13	$5.02^e$	1.76	0.02	$2.1 \pm 0.14^o$	Bmrs
SwSt1	1.59	-6.72	$2^f$	$5.6^m$	0.03	$8 \pm 0.6^p$	S
Hu 2-1	51.48	+9.68	$2.38^g$	2.06	0.01	$0.68 \pm 0.09^p$	Bmps
M 3-35	71.63	-2.36	$2.4^h$	1.65	0.01	$2.5 \pm 0.3^p$	Bamps
NGC 7293	36.16	-57.12	$0.2^i$	$970^m$	0.47	$0.03^q$	Bmprs
IC 4997	58.33	-10.98	$5^j$	1.72	0.02	$3.7 \pm 0.06^j$	Bmps
BD+30 $^\circ$ 3639	64.79	+5.02	$1.5^k$	4.93	0.02	$2.65 \pm 0.09^k$	Eamrs

NOTE—<sup>a</sup> Gómez et al. (2008); <sup>b</sup> Gathier et al. (1986); <sup>c</sup> Pottasch & Surendiranath (2005); <sup>d</sup> Morisset & Georgiev (2009); <sup>e</sup> Vickers et al. (2015); <sup>f</sup> De Marco et al. (2001); <sup>g</sup> Santander-García et al. (2022); <sup>h</sup> Weinberger (1989); <sup>i</sup> Luri et al. (2018); <sup>j</sup> Ouyang et al. (2022); <sup>k</sup> Ouyang et al. (2023); <sup>l</sup> Bojičić et al. (2021); <sup>m</sup> HASH; <sup>n</sup> Rodríguez & Moran (1982); <sup>o</sup> Taylor et al. (1990); <sup>p</sup> Gussie & Taylor (1995); <sup>q</sup> Rodríguez et al. (2002).

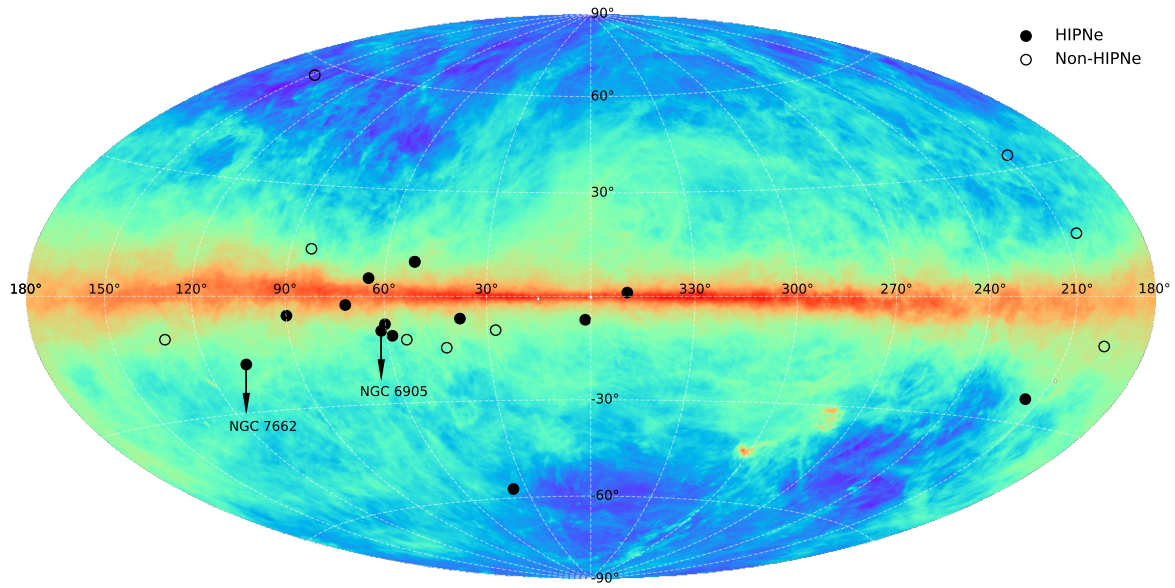


**Figure 1.** Positions of the our PN sample and the known HIPNe retrieved from the literature in the Galactic coordinate system. The filled circles represent HIPNe, with newly detected sources in this observation labeled by their names. The open circles represent PNe where H I is not detected in our observations. The background is an all-sky H I column density map integrated over the full velocity range of  $-600 \text{ km s}^{-1} \leq v_{\text{LSR}} \leq 600 \text{ km s}^{-1}$ , adopted from [HI4PI Collaboration et al. \(2016\)](#).

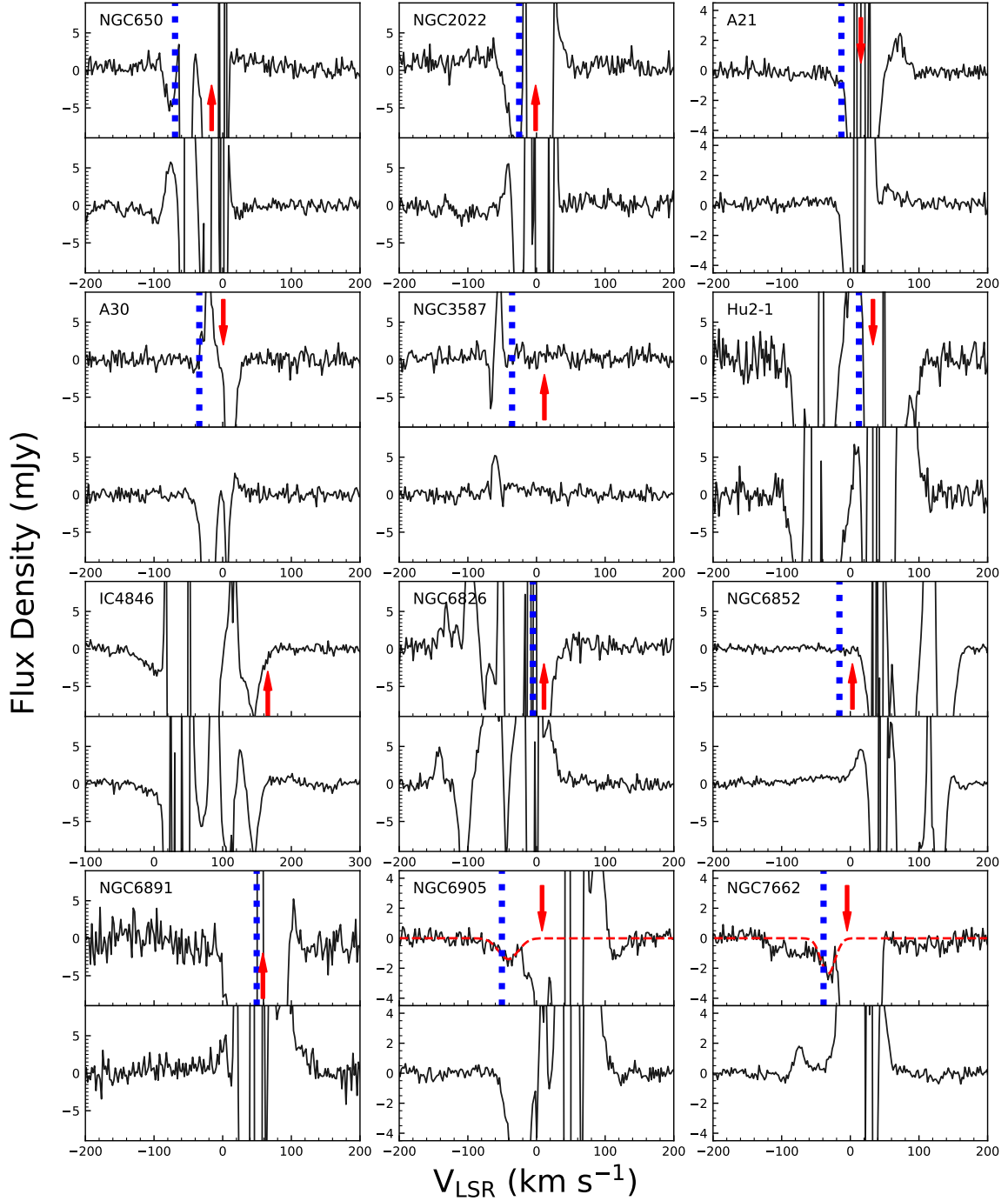


**Figure 2.** H I spectra of PNe. For each subfigure, the top and bottom panels show the ON–OFF and OFF–OFF spectra, respectively. The arrows mark the systemic velocity position the PNe. The vertical dotted line indicates the velocities of the blue end of optical emission lines ([N II] or H $\alpha$  lines), with the exception of IC 4846, where no such emission lines are found in the literature. A fitting to the potential circumstellar H I absorption is shown by the dashed curves.

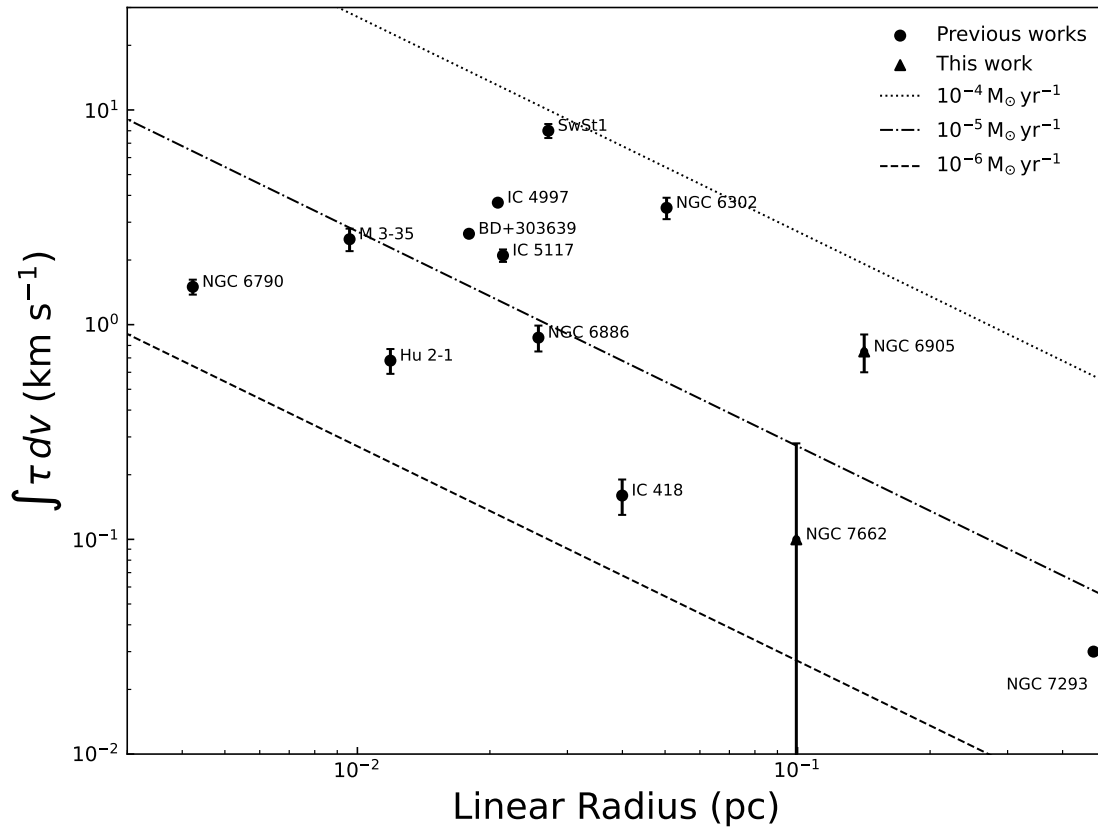


**Figure 3.** Integrated H I optical depth versus linear radius of the ionized regions. The diagonal lines represent the results derived from theoretical calculations based on different mass-loss rates (as shown in the upper right corner).